THE JOURNAL OF PHYSICAL CHEMISTRY LETTERS
A JOURNAL OF THE AMERICAN CHEMICAL SOCIETY

pubs.acs.org/JPCL

Letter

# Scalable High-Pressure Synthesis of $sp^2$–$sp^3$ Carbon Nanoribbon via [4 + 2] Polymerization of 1,3,5-Triethynylbenzene

Yapei Li, Xingyu Tang, Peijie Zhang, Yida Wang, Xin Yang, Xuan Wang, Kuo Li, Yajie Wang, Ningning Wu, Mingxue Tang, Junfeng Xiang, Xiaohuan Lin, Hyun Hwi Lee, Xiao Dong, Haiyan Zheng,* and Ho-kwang Mao

Cite This: *J. Phys. Chem. Lett.* 2021, 12, 7140–7145

Read Online

ACCESS | Metrics & More | Article Recommendations | Supporting Information

**ABSTRACT:** Pressure-induced polymerization of aromatics is an effective method to construct extended carbon materials, including the diamond-like nanothread and graphitic structures, but the reaction pressure of phenyl is typically around 20 GPa and too high to be applied for large-scale preparation. Here by introducing ethynyl to phenyl, we obtained a $sp^2$–$sp^3$ carbon nanoribbon structure by compressing 1,3,5-triethynylbenzene (TEB), and the reaction pressure of phenyl was successfully decreased to 4 GPa, which is the lowest reaction pressure of aromatics at room temperature. Using experimental and theoretical methods, we figured out that the ethynylphenyl of TEB undergoes [4 + 2] dehydro-Diels–Alder (DDA) reaction with phenyl upon compression at an intermolecular C···C distance above 3.3 Å, which is much longer than those of benzene and acetylene. Our research suggested that the DDA reaction between ethynylphenyl and phenyl is a promising route to decrease the reaction pressure of aromatics, which allows the scalable high-pressure synthesis of nanoribbon materials.

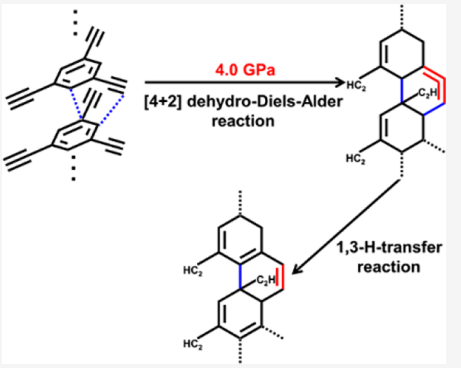


Pressure-induced polymerization (PIP) of aromatics is a robust method to synthesize novel carbon materials.[1−3] By compression of benzene to ∼20 GPa at room temperature, ultrathin one-dimensional (1-D) $sp^3$ carbon nanothreads were obtained, with a stiff diamond-like structure.[4] Introducing functional groups and heteroatoms can modify the reaction process, structure, and properties of the product; hence, a variety of aromatics were investigated, like furan,[5,6] pyrrole,[7] thiophene,[8,9] pyridine,[10,11] aniline,[12] pyrimidine,[13,14] triazine,[13,15,16] 2,4,6-tricyano-1,3,5-triazine (TCT),[17] benzene–hexafluorobenzene cocrystal,[18] and benzene–acetylene cocrystal.[19] New materials including 1-D N- or O-doped nanothreads, 2-D F-doped graphane, and extended nitrogen-rich amorphous hydrogenated carbon (*a*-C:H:N) were thus obtained. These materials greatly expanded the family of carbon materials. However, the required pressures for the PIP of aromatics are typically around 20 GPa at room temperature, with the lowest one at 10 GPa for furan, which is too high to be applied for large-scale preparation and prevent further investigation.

In comparison, alkynes often polymerize in a solid at much lower pressure. Acetylene polymerizes at ∼4 GPa at room temperature and produce polyacetylene and graphane.[20−22] $C_2I_2$ also polymerizes at 4 GPa and forms conjugated iodocarbon materials.[23] This reminds us that ethynyl may help to decrease the reaction pressure of the aromatics. Although in phenylacetylene ethynyl and phenyl did not react synergistically,[24] very recently, we found that the phenyl of diphenylbutadiyne reacts with ethynylphenyl at ∼10 GPa via a [4 + 2] dehydro-Diels–Alder (DDA) reaction and produces crystalline graphitic nanoribbon.[25] This suggests that the cycloaddition of phenyl and ethynyl in PIP is still promising and worthy to be explored. In this work, we investigated the PIP of crystalline 1,3,5-triethynylbenzene (TEB) and found the phenyl undergoes [4 + 2] DDA reaction with neighbored ethynylphenyl to form 1-D nanoribbon at 4 GPa. This is an unprecedented low pressure for aromatics to react under room temperature, which can be applied for large-scale synthesis, and PIP-TEB is hence the most easily scalable synthesized 1-D nanoribbon from PIP of aromatics.

At room temperature, the Raman spectra of TEB keep their profile upon compression, and no new peak appears below 3.0 GPa (Figure 1a), with assignments in Figure S1. At 4 GPa, the signal of TEB disappeared with fluorescence enhanced dramatically, suggesting the reaction begins. Four new bands appeared at 654, 868, 1241, and 1511 $cm^{-1}$. The latter two are attributed to $sp^3$ C–C and $sp^2$ C=C stretching modes,

**Received:** June 17, 2021
**Accepted:** July 19, 2021







https://doi.org/10.1021/acs.jpclett.1c01945
*J. Phys. Chem. Lett.* 2021, 12, 7140–7145

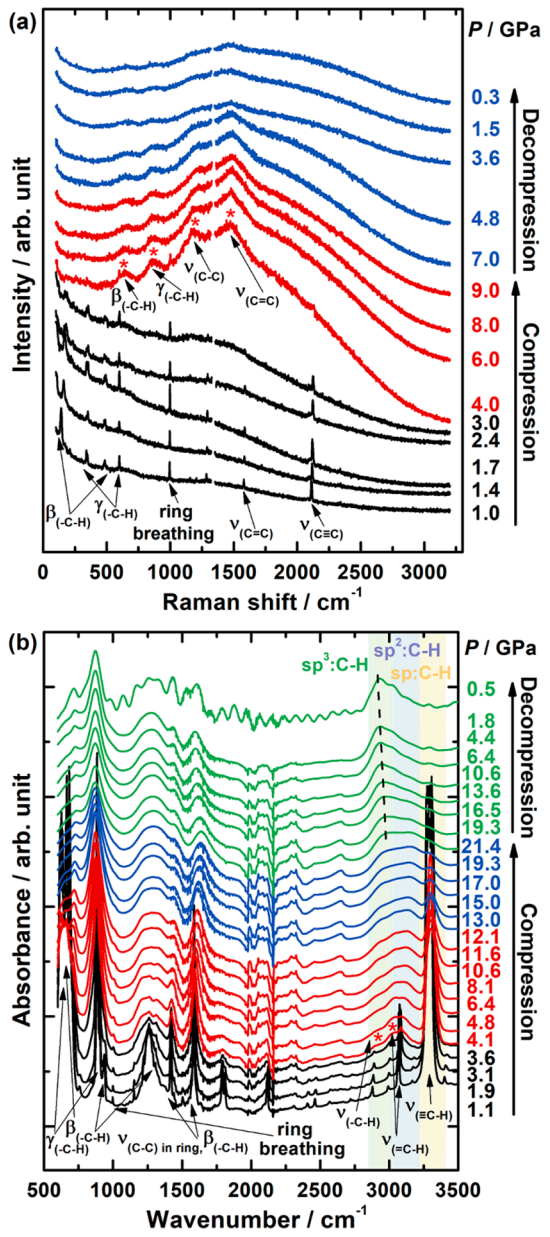


**Figure 1.** (a) In situ Raman and (b) IR spectra of TEB during compression and decompression. The asterisks indicate the new peaks. $\nu$ for stretching, $\gamma$ for the out-of-plane bending, and $\beta$ for the in-plane bending.

respectively, indicating that TEB underwent PIP reaction and formed C−C and C═C bonds. The pressure dependences of Raman frequencies are shown in Figure S2, which clearly shows the chemical reaction occurring at 4 GPa.

In situ IR spectra were also measured to avoid fluorescence and possible photoreaction (Figure 1b), and the assignments of the selected IR modes are shown in Figure S3. Similar to Raman results, at 4.1 GPa, the absorptions from the phenyl, including the C−H stretching ($\nu_{(=C-H)}$) at 3082 cm$^{-1}$, the C−C stretching ($\nu_{(C-C)}$) in ring and C−H in-plane bending vibration ($\beta_{(-C-H)}$) located at 1590, 1422, and 1262 cm$^{-1}$, and the C−H out-of-plane bending ($\gamma_{(-C-H)}$) vibration at 884 cm$^{-1}$ were weakened obviously and then disappeared gradually (Figure 1b and Figure S4). Meanwhile, the intensities of C−H stretching of the ethynyl moiety (3296 cm$^{-1}$), the $\beta_{(-C-H)}$ at 664 and 682 cm$^{-1}$, and the $\gamma_{(-C-H)}$ at 622 cm$^{-1}$ also decreased obviously at 4.1 GPa (Figure 1b and Figure S4). Simultaneously, the sp$^3$ C−H (2901 cm$^{-1}$, asterisked in Figure 1b) and sp$^2$ C−H stretching (3035 cm$^{-1}$, asterisked in Figure 1b) appeared. These series of transformations clearly demonstrated that phenyl and ethynyl reacted simultaneously to produce sp$^3$ C−H and C═C. It must be noted that 4.1 GPa is much lower than any of the reported aromatics' reaction pressure, which is ascribed to the DDA reaction route of ethynylphenyl and phenyl as discussed below.

To understand the structure evolution of TEB under high pressure, we performed in situ X-ray diffraction (XRD) up to 4.6 GPa. TEB crystal has a monoclinic structure (space group $C2/c$, $a$ = 18.4 Å, $b$ = 3.7 Å, $c$ = 22.4 Å, and $\beta$ = 108.3°) at ambient pressure, and the molecules stack in column along the $b$-axis.[26] With increasing pressure, all the XRD peaks were broadened, shifted to low $d$-spacing, and almost disappeared above 3.6 GPa corresponding to PIP (Figure 2a). When released to 0 GPa, only three weak peaks centered at $2\theta$ = 3.7°,

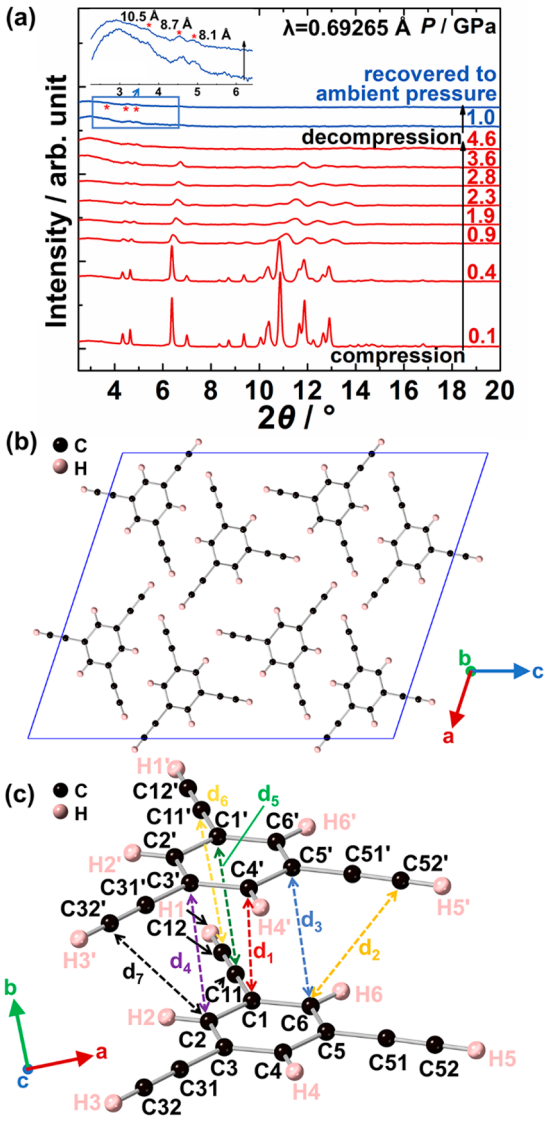


**Figure 2.** (a) In situ XRD patterns of TEB during compression and decompression. The asterisks stand for the new peaks of the product. (b) Crystal structure of TEB optimized at 3.6 GPa. (c) Intermolecular C···C distances at 3.6 GPa.



https://doi.org/10.1021/acs.jpclett.1c01945
J. Phys. Chem. Lett. 2021, 12, 7140−7145

4.5°, and 4.9° ($d$ = 10.5, 8.7, and 8.1 Å) were observed. These peaks were not from the reactant, which indicated that some crystalline product was produced irreversibly in the experimental time scale (tens of minutes). The lattice parameters during compression were obtained by Rietveld refinement (Figure S5a). The $P-V$ relationship of TEB was then fitted by one third-order Birch−Murnaghan equation of state,[27] with $V_0$ = 1767 ± 23 Å$^3$, $B_0$ = 10 ± 3 GPa, and $B_1$ = 5 ± 3 (Figure S5b).

The crystal structure of TEB closed to reaction pressure was investigated by performing the Rietveld refinement on the XRD data at 3.6 GPa (Figure S5c). The obtained structure was then optimized by density functional theory (DFT) calculation to get accurate atomic positions, with the lattice parameters fixed at the experimental values ($a$ = 18.4 Å, $b$ = 3.7 Å, $c$ = 22.4 Å, and $\beta$ = 108.3°). As shown in Figure 2b, the TEB molecules are parallelly stacked in columns along [010] with the molecular plane tilt 27.7° away from the (010) plane. Hence, the molecular center is approximately above the C1′−C11′ bond of one neighboring molecule and below H4′ of the other neighboring molecule (Figure 2c). The typical intermolecular C···C distances are $d_1$ = 3.39 Å, $d_2$ = 3.89 Å, $d_{3,4,5}$ = 3.30 Å, $d_6$ = 3.33 Å, and $d_7$ = 4.10 Å (Figure 2c). Upon comparison with the critical PIP distance of aromatics (2.8 Å)[18,28] and alkyne (2.9−3.1 Å)[22,29,30] at room temperature without a thermal effect correction (details listed in Table S1), the C···C distances of TEB closed to the reaction pressure are significantly larger. This suggests that the phenyl and ethynyl are not likely to react separately as that in PIP of benzene or acetylene, and another reaction path should be concluded. This is also different from the case in TCT,[17] in which the cyano is proposed to trimerize under 10.5 GPa at room temperature with the aromatic ring unreacted.

A meta-dynamic calculation (M-D) was then performed to simulate the PIP process at 4 GPa and 300 K starting from the crystal structure at 3.6 GPa. Most of the reactions occurred in the third step of M-D; hence, we optimized the product structure obtained from this step (meta-3) by DFT calculations. The optimization results show eight infinite ribbons with four kinds of structures in one unit cell, and they are referred as 3-1, 3-2, 3-4, and 3-5, as shown in Figure 3a,b. At this step all the products contain allene, which is not detected in IR spectra (supposed at 1950 cm$^{-1}$, asymmetric stretching vibration) or $^{13}$C nuclear magnetic resonance (NMR) data (210 ppm) mentioned later, and should not be the final product due to its instability. Thus, on the basis of the carbon skeletal, we rearranged the distribution of H via 1,3-H-transfer reaction and optimized the structure again at 0 GPa. The final product, meta-3-H, including one 3-1-H, five 3-2-H, one 3-4-H, and one 3-5-H infinite ribbons, is shown in Figure 3a,b. To understand the processes of PIP, we reviewed the bonding routes in the M-D results. In the dominating (5/8) structure 3-2, C52′ on ethynyl bonds to C6 on the phenyl group. After several steps with the shortest 4 fs and longest 62 fs, C1 bonds to C4′ and forms polymer 3-2. The time gap between formation of these two new bonds is extremely short, indicating a synergetic bonding process between ethynylphenyl and ethynyl,[31] and hence a [4 + 2] DDA reaction between C4′−C5′−C51′−C52′ (ethynylphenyl as a diene) and C1−C6 (phenyl as a dienophile) can be concluded. A similar [4 + 2] DDA reaction also happened between C4′−C3′−C31′−C32′ and C1−C2, forming 3-5 in a mirrored geometry compared to 3-2. 3-1 can be considered as a further reaction of 3-2 with

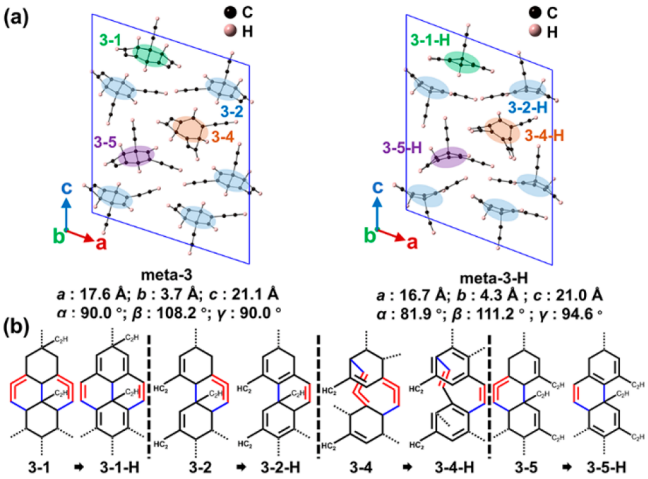


**Figure 3.** Structure models of the product. (a) Crystal structures of meta-3 and meta-3-H. 3-1(-H), 3-2(-H), 3-4(-H), and 3-5(-H) are distinguished by green, blue, orange, and purple coverings, respectively. (b) Models of ribbons (3-1, 3-1-H, 3-2, 3-2-H, 3-4, 3-4-H, 3-5, and 3-5-H). New bonds are in blue, and double bonds are in red.

C32′ and C2 bonded. Additionally, there is another bonding route between ethynylphenyl and phenyl (3-4 in Figure 3) with 1/8 of the ribbons in one unit cell. This low content may be due to the less stability of the 10-membered ring compared with the six-membered ring formed through DDA routes. The M-D results show that the PIP of TEB is nonuniform but with DDA reaction as a dominating route. The product models including the 3-1-H, 3-2-H, 3-4-H, and 3-5-H were proposed (Figure 3b) and confirmed by the following investigation, though other models for the product are not excluded.

To demonstrate the structure of product experimentally, tens of milligrams of PIP-TEB were synthesized at 5 GPa by using the Paris−Edinburgh (PE) press (referred as PE5). The product was washed with dichloromethane to remove unreacted TEB and oligomers. ∼20 mg of PE5 can be obtained in 1.5 h or 30−40 mg in 4−5 h in one compression. The lab XRD results show five peaks at $2\theta$ = 8.5° (10.5 Å), 10.2° (8.51 Å), 11.03° (8.02 Å), 15.8° (5.50 Å), and 17.2° (5.06 Å) (Figure 4a), consistent with the product recovered from the in situ XRD experiments (10.5, 8.7, and 8.1 Å). The distribution of these peaks of PE5 was similar to the 002, 200, 20$\bar{2}$, 202, and 004 peaks of its precursor TEB powder. On the basis of a topochemical reaction process, we traced XRD peaks from TEB to PE5 with its Miller index unchanged and then calculated and refined the cell parameters of PE5, with $a$ = 18.3 Å, $c$ = 21.9 Å, and $\beta$ = 106.9°. The Le Bail fitting plot of PE5 is shown in Figure S6. $b$ cannot be determined directly due to lacking of $hkl$ ($k \neq 0$) peaks, which indicates the disordering along the $b$-axis and is consistent with the pressure-induced reaction occurring along the $b$-axis.

Under a high-resolution transmission electron microscope (TEM), PE5 shows obvious lattice stripes with a $d$-spacing ∼7.86 Å, which fits well with the 200 peak in lab XRD results (Figure 4b). In the selected area electron diffraction (SAED) pattern, two-dimensional ordering was identified, and the diffractions were indexed as 200 ($d_{200}$ = 8.0 Å) and 002 ($d_{002}$ = 10.2 Å) (Figure 4c). These results are consistent with the theoretically predicted structure as shown in Figures 3a and 4d.



https://doi.org/10.1021/acs.jpclett.1c01945
J. Phys. Chem. Lett. 2021, 12, 7140−7145

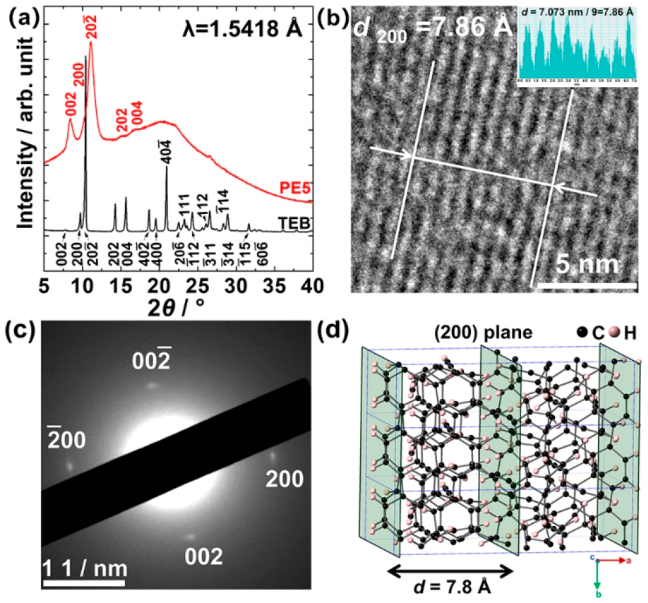


**Figure 4.** (a) Lab XRD, (b) high-resolution transmission electron microscopy (TEM) and (c) selected area electron diffraction (SAED) pattern of PE5. (d) Side view of the ribbons (meta-3-H) along the *c*-axis. The (200) plane is represented in green, with a *d*-spacing of 7.8 Å.

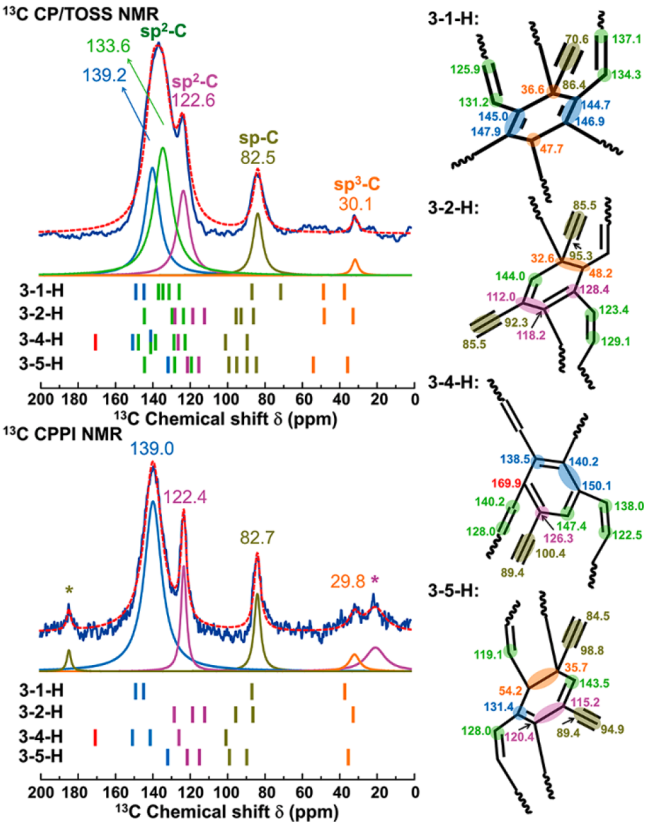


**Figure 5.** $^{13}$C CP/TOSS NMR spectrum and CPPI NMR spectrum of PE5. Vertical bars represent the calculated chemical shift. The blue solid and red dashed line represent experimental results and the cumulative fit peak, respectively. The asterisks represent spinning side bands.

The Raman and IR spectra of PE5 evidenced that the C−C and C═C groups were present in PE 5 (Figure S7). Meanwhile, the C−H stretching of the ethynyl moiety can be still observed in the IR spectrum of PE5, which is consistent with the proposed models. We simulated the IR spectrum of the proposed models, which fits the experimental result very well (Figure S7b).

The high-resolution solid state magic angle spinning nuclear magnetic resonance (MAS NMR) spectra of PE5 are shown in Figure 5 with that of pristine TEB in Figure S8 for reference. Compared to the $^{13}$C cross-polarization with total suppression of side bands (CP/TOSS) spectrum of TEB, a new peak centered at 30.1 ppm and broad peaks in the 100−160 ppm range were observed in PE5, indicating its complex carbon environment (Figure 5). Peaks at 139.2, 133.6, and 122.6 ppm are attributed to sp$^2$ C, and those at 82.5 and 30.1 ppm are ascribed to sp C and newly formed sp$^3$ C, respectively. Then, the $^{13}$C cross-polarization/polarization inversion (CPPI) NMR spectrum was collected to distinguish the $-CH_2$, CH, and C/$CH_3$ groups in PE5 which show negative, zero, and positive peaks, respectively. Upon comparison of these two spectra, four positive peaks at 29.8, 82.7, 122.4, and 139.0 ppm are shown in the CPPI spectrum, while the peak centered at 133.6 ppm in the CP/TOSS spectrum disappeared (Figure S9). Thus, the peak centered at 30.1 ppm observed in CP/TOSS should be attributed to the quaternary carbon because there is no methyl carbon ($-CH_3$) observed in PE5. The peaks centered at 139.2 and 122.6 ppm are corresponding to the sp$^2$ C bonded to three carbon atoms, and the peak at 133.6 ppm is for the sp$^2$ CH group. The experiment results of PE5 are consistent with the simulation NMR results based on the 3-1-H, 3-2-H, 3-4-H, and 3-5-H models, and the assignments of the carbon environments are shown in Figure 5. It is worthy to mention that the 3-4-H does not contain sp$^3$ C, and the peak at 169.9 ppm was not observed either, which suggests a low content. This also confirmed that the 3-1-H, 3-2-H, and 3-5-H produced from the [4 + 2] DDA reaction is the dominating reaction routes.

The [4 + 2] DDA reaction path of TEB observed in this work is completely different from that of phenylacetylene.[24] The extra two ethynyls results in obvious synergetic effect, which decreased the reaction pressure significantly. The critical reaction distance through [4 + 2] route is above 3.3 Å, in contrast to 2.9−3.1 Å for alkynes and 2.8 Å for aromatics.[18,22,28−30] This suggests that the critical distance is not only functional-group-sensitive but also path-sensitive. Additionally, the decreasing of reaction pressure not only allows large-scale synthesis but also avoids the severe local stress under higher pressure and hence improves the crystallinity.

In summary, we investigated the reaction process and product structures of TEB under high pressure systematically by combination of experiment and simulation methods. TEB polymerizes at 4 GPa under room temperature, which is much lower than any of reported aromatics' reaction pressure under room temperature, and can be applied for scalable high-pressure synthesis. The obtained product has unprecedented 1-D nanoribbons structure with sp, sp$^2$, and sp$^3$ carbons. We conclude that TEB experienced a [4 + 2] dehydro-Diels−Alder reaction under high pressure with ethynylphenyl as a diene and phenyl as a dienophile. Our study demonstrated that the synergetic reaction of ethynyl and phenyl can help to decrease the polymerization pressure and thus improve the crystallinity


https://doi.org/10.1021/acs.jpclett.1c01945
J. Phys. Chem. Lett. 2021, 12, 7140−7145

of the polymerized product efficiently, which sheds light on the large-scale high-pressure synthesis of 1-D carbon nanoribbons.

## ■ ASSOCIATED CONTENT

### Supporting Information

The Supporting Information is available free of charge at https://pubs.acs.org/doi/10.1021/acs.jpclett.1c01945.

Details of materials and methods; assignments of Raman modes of TEB at ambient pressure, room temperature; Raman shifts as a function of pressure ranging from 100 to 1650 $cm^{-1}$ and 2100−2200 $cm^{-1}$; assignments of IR modes of TEB at ambient pressure, room temperature; 3D-plot of in situ IR spectra in the ranges of 600−1800 $cm^{-1}$ and 2750−3550 $cm^{-1}$; evolution of corresponding lattice parameters of TEB from 0.1 to 3.6 GPa; $P-V$ relationship of TEB fitting by the third-order Birch−Murnaghan equation of state, with $V_0$ = 1767 ± 23 $Å^3$, $B_0$ = 10 ± 3 GPa, and $B_1$ = 5 ± 3; Rietveld refinement plot of TEB at 3.6 GPa; Le Bail fitting plot of PE5 by JANA2006; Raman spectrum, experimental and calculated IR spectra of PE5; $^{13}C$ CP/TOSS NMR spectrum of TEB; comparison of $^{13}C$ CP/TOSS and CPPI NMR spectra of PE5 (PDF)

## ■ AUTHOR INFORMATION


### Corresponding Author

**Haiyan Zheng** − *Center for High Pressure Science and Technology Advanced Research, Beijing 100094, China;* orcid.org/0000-0002-4727-5912; Email: zhenghy@hpstar.ac.cn

### Authors

**Yapei Li** − *Center for High Pressure Science and Technology Advanced Research, Beijing 100094, China*

**Xingyu Tang** − *Center for High Pressure Science and Technology Advanced Research, Beijing 100094, China*

**Peijie Zhang** − *Center for High Pressure Science and Technology Advanced Research, Beijing 100094, China;* orcid.org/0000-0001-6355-5482

**Yida Wang** − *Center for High Pressure Science and Technology Advanced Research, Beijing 100094, China*

**Xin Yang** − *Center for High Pressure Science and Technology Advanced Research, Beijing 100094, China*

**Xuan Wang** − *Center for High Pressure Science and Technology Advanced Research, Beijing 100094, China*

**Kuo Li** − *Center for High Pressure Science and Technology Advanced Research, Beijing 100094, China;* orcid.org/0000-0002-4859-6099

**Yajie Wang** − *Center for High Pressure Science and Technology Advanced Research, Beijing 100094, China*

**Ningning Wu** − *Center for Physicochemical Analysis and Measurement, Institute of Chemistry, Chinese Academy of Sciences, Beijing 100190, China*

**Mingxue Tang** − *Center for High Pressure Science and Technology Advanced Research, Beijing 100094, China;* orcid.org/0000-0002-7282-4100

**Junfeng Xiang** − *Center for Physicochemical Analysis and Measurement, Institute of Chemistry, Chinese Academy of Sciences, Beijing 100190, China*

**Xiaohuan Lin** − *Center for High Pressure Science and Technology Advanced Research, Beijing 100094, China*

**Hyun Hwi Lee** − *Pohang Accelerator Laboratory, POSTECH, Pohang 790-784, Republic of Korea*

**Xiao Dong** − *Key Laboratory of Weak-Light Nonlinear Photonics, School of Physics, Nankai University, Tianjin 300071, China*

**Ho-kwang Mao** − *Center for High Pressure Science and Technology Advanced Research, Beijing 100094, China*

Complete contact information is available at: https://pubs.acs.org/10.1021/acs.jpclett.1c01945


### Notes

The authors declare no competing financial interest.

## ■ ACKNOWLEDGMENTS

The authors acknowledge the support of the National Natural Science Foundation of China (NSFC) (Grants 21875006, 21771011, and 22022101) and the National Key Research and Development Program of China (2019YFA0708502). This research used resources of Pohang Accelerator Laboratory, Beijing Synchrotron Radiation Facility and Shanghai Synchrotron Radiation Facility. The authors thank Drs. Yang Ren, He Lin, Manrong Li, Hongkai Gu, and Yifeng Han for their kind help with pair distribution function (PDF) measurements and discussions.

## ■ REFERENCES


(1) Yang, X.; Wang, X.; Wang, Y.; Li, K.; Zheng, H. From Molecules to Carbon Materials-High Pressure Induced Polymerization and Bonding Mechanisms of Unsaturated Compounds. *Crystals* **2019**, *9* (10), 490.

(2) Wang, X.; Li, K.; Zheng, H.; Zhang, P. Chemical Reactions of Molecules under High Pressure. *Chem. Bull.* **2019**, *82* (5), 387−398.

(3) Mao, H.-K.; Chen, B.; Chen, J.; Li, K.; Lin, J.-F.; Yang, W.; Zheng, H. Recent Advances in High-Pressure Science and Technology. *Matter Radiat. at Extremes* **2016**, *1* (1), 59−75.

(4) Li, X.; Baldini, M.; Wang, T.; Chen, B.; Xu, E.-S.; Vermilyea, B.; Crespi, V. H.; Hoffmann, R.; Molaison, J. J.; Tulk, C. A.; et al. Mechanochemical Synthesis of Carbon Nanothread Single Crystals. *J. Am. Chem. Soc.* **2017**, *139* (45), 16343−16349.

(5) Ceppatelli, M.; Santoro, M.; Bini, R.; Schettino, V. High Pressure Reactivity of Solid Furan Probed by Infrared and Raman Spectroscopy. *J. Chem. Phys.* **2003**, *118* (3), 1499−1506.

(6) Huss, S.; Wu, S.; Chen, B.; Wang, T.; Gerthoffer, M. C.; Ryan, D. J.; Smith, S. E.; Crespi, V. H.; Badding, J. V.; Elacqua, E. Scalable Synthesis of Crystalline One-Dimensional Carbon Nanothreads through Modest-Pressure Polymerization of Furan. *ACS Nano* **2021**, *15* (3), 4134−4143.

(7) Li, W.; Duan, D.; Huang, X.; Jin, X.; Yang, X.; Li, S.; Jiang, S.; Huang, Y.; Li, F.; Cui, Q.; et al. Pressure-Induced Diversity of $\pi$-Stacking Motifs and Amorphous Polymerization in Pyrrole. *J. Phys. Chem. C* **2014**, *118* (23), 12420−12427.

(8) Pruzan, P.; Chervin, J. C.; Forgerit, J. P. Chemical and Phase Transformations of Thiophene at High Pressures. *J. Chem. Phys.* **1992**, *96* (1), 761−767.

(9) Biswas, A.; Ward, M. D.; Wang, T.; Zhu, L.; Huang, H.-T.; Badding, J. V.; Crespi, V. H.; Strobel, T. A. Evidence for Orientational Order in Nanothreads Derived from Thiophene. *J. Phys. Chem. Lett.* **2019**, *10* (22), 7164−7171.

(10) Li, X.; Wang, T.; Duan, P.; Baldini, M.; Huang, H.-T.; Chen, B.; Juhl, S. J.; Koeplinger, D.; Crespi, V. H.; Schmidt-Rohr, K.; et al. Carbon Nitride Nanothread Crystals Derived from Pyridine. *J. Am. Chem. Soc.* **2018**, *140* (15), 4969−4972.

(11) Fanetti, S.; Santoro, M.; Alabarse, F.; Enrico, B.; Bini, R. Modulating the H-Bond Strength by Varying the Temperature for the High Pressure Synthesis of Nitrogen Rich Carbon Nanothreads. *Nanoscale* **2020**, *12* (8), 5233−5242.

(12) Nobrega, M. M.; Teixeira-Neto, E.; Cairns, A. B.; Temperini, M. L. A.; Bini, R. One-Dimensional Diamondoid Polyaniline-like Nanothreads from Compressed Crystal Aniline. *Chem. Sci.* **2018**, *9* (1), 254−260.
(13) Li, S.; Li, Q.; Xiong, L.; Li, X.; Li, W.; Cui, W.; Liu, R.; Liu, J.; Yang, K.; Liu, B.; et al. Effect of Pressure on Heterocyclic Compounds: Pyrimidine and s-Triazine. *J. Chem. Phys.* **2014**, *141* (11), 114902.
(14) Patyk, E.; Podsiadło, M.; Katrusiak, A. CH···N Bonds and Dynamics in Isostructural Pyrimidine Polymorphs. *Cryst. Growth Des.* **2015**, *15* (8), 4039−4044.
(15) Citroni, M.; Fanetti, S.; Bini, R. Pressure and Laser-Induced Reactivity in Crystalline s-Triazine. *J. Phys. Chem. C* **2014**, *118* (19), 10284−10290.
(16) Citroni, M.; Fanetti, S.; Bazzicalupi, C.; Dziubek, K.; Pagliai, M.; Nobrega, M. M.; Mezouar, M.; Bini, R. Structural and Electronic Competing Mechanisms in the Formation of Amorphous Carbon Nitride by Compressing s-Triazine. *J. Phys. Chem. C* **2015**, *119* (51), 28560−28569.
(17) Fanetti, S.; Nobrega, M. M.; Dziubek, K.; Citroni, M.; Sella, A.; McMillan, P. F.; Hanfland, M.; Bini, R. Structure and Reactivity of 2,4,6-Tricyano-1,3,5-Triazine under High-Pressure Conditions. *CrystEngComm* **2019**, *21* (30), 4493−4500.
(18) Wang, Y.; Dong, X.; Tang, X.; Zheng, H.; Li, K.; Lin, X.; Fang, L.; Sun, G.; Chen, X.; Xie, L.; et al. Pressure-Induced Diels-Alder Reactions in $C_6H_6$-$C_6F_6$ Cocrystal towards Graphane Structure. *Angew. Chem., Int. Ed.* **2019**, *58* (5), 1468−1473.
(19) Ward, M. D.; Huang, H.-T.; Zhu, L.; Biswas, A.; Popov, D.; Badding, J. V.; Strobel, T. A. Chemistry through Cocrystals: Pressure-Induced Polymerization of $C_2H_2$·$C_6H_6$ to an Extended Crystalline Hydrocarbon. *Phys. Chem. Chem. Phys.* **2018**, *20* (10), 7282−7294.
(20) Aoki, K.; Usuba, S.; Yoshida, M.; Kakudate, Y.; Tanaka, K.; Fujiwara, S. Raman Study of the Solid-State Polymerization of Acetylene at High Pressure. *J. Chem. Phys.* **1988**, *89* (1), 529−534.
(21) Trout, C. C.; Badding, J. V. Solid State Polymerization of Acetylene at High Pressure and Low Temperature. *J. Phys. Chem. A* **2000**, *104* (34), 8142−8145.
(22) Sun, J.; Dong, X.; Wang, Y.; Li, K.; Zheng, H.; Wang, L.; Cody, G. D.; Tulk, C. A.; Molaison, J. J.; Lin, X.; et al. Pressure-Induced Polymerization of Acetylene: Structure-Directed Stereoselectivity and a Possible Route to Graphane. *Angew. Chem., Int. Ed.* **2017**, *56* (23), 6553−6557.
(23) Ward, M. D.; Huang, H.-T.; Zhu, L.; Popov, D.; Strobel, T. A. High-Pressure Behavior of $C_2I_2$ and Polymerization to a Conductive Polymer. *J. Phys. Chem. C* **2019**, *123* (18), 11369−11377.
(24) Santoro, M.; Ciabini, L.; Bini, R.; Schettino, V. High-Pressure Polymerization of Phenylacetylene and of the Benzene and Acetylene Moieties. *J. Raman Spectrosc.* **2003**, *34* (7−8), 557−566.
(25) Zhang, P.; Tang, X.; Wang, Y.; Wang, X.; Gao, D.; Li, Y.; Zheng, H.; Wang, Y.; Wang, X.; Fu, R.; et al. Distance-Selected Topochemical Dehydro-Diels-Alder Reaction of 1,4-Diphenylbutadiyne toward Crystalline Graphitic Nanoribbons. *J. Am. Chem. Soc.* **2020**, *142* (41), 17662−17669.
(26) Weiss, H.-C.; Bläser, D.; Boese, R.; Doughan, B. M.; Haley, M. M. C-H···$\pi$ Interactions in Ethynylbenzenes: the Crystal Structures of Ethynylbenzene and 1,3,5-Triethynylbenzene, and a Redetermination of the Structure of 1,4-Diethynylbenzene. *Chem. Commun.* **1997**, *18*, 1703−1704.
(27) Birch, F. Finite Strain Isotherm and Velocities for Single-Crystal and Polycrystalline NaCl at High Pressures and 300°K. *J. Geophys. Res.* **1978**, *83* (B3), 1257−1268.
(28) Ciabini, L.; Santoro, M.; Gorelli, F. A.; Bini, R.; Schettino, V.; Raugei, S. Triggering Dynamics of the High-Pressure Benzene Amorphization. *Nat. Mater.* **2007**, *6* (1), 39−43.
(29) Zheng, H.; Wang, L.; Li, K.; Yang, Y.; Wang, Y.; Wu, J.; Dong, X.; Wang, C.-H.; Tulk, C. A.; Molaison, J. J.; et al. Pressure Induced Polymerization of Acetylide Anions in $CaC_2$ and $10^7$ Fold Enhancement of Electrical Conductivity. *Chem. Sci.* **2017**, *8* (1), 298−304.
(30) Han, J.; Tang, X.; Wang, Y.; Wang, Y.; Han, Y.; Lin, X.; Dong, X.; Lee, H. H.; Zheng, H.; Li, K.; et al. Pressure-Induced Polymerization of Monosodium Acetylide: a Radical Reaction Initiated Topochemically. *J. Phys. Chem. C* **2019**, *123* (50), 30746−30753.
(31) Black, K.; Liu, P.; Xu, L.; Doubleday, C.; Houk, K. N. Dynamics, Transition States, and Timing of Bond Formation in Diels-Alder Reactions. *Proc. Natl. Acad. Sci. U. S. A.* **2012**, *109* (32), 12860−12865.


https://doi.org/10.1021/acs.jpclett.1c01945
J. Phys. Chem. Lett. 2021, 12, 7140−7145